ON THE NUMERICAL IMPLEMENTATION OF ELASTO-PLASTIC CONSTITUTIVE EQUATIONS FOR METAL FORMING

TUDOR BĂLAN

Abstract. This paper is devoted to the time integration of elasto-plastic constitutive models, in view of their implementation in finite element software for the simulation of metal forming processes. Both implicit and explicit time integration schemes are reviewed and presented in algorithmic form. The incremental kinematics are also treated, so that the proposed algorithms can be used stand-alone, outside a finite element code, or they can serve to implement non-classical incremental kinematics. Full algorithms are provided, along with examples of application to non-monotonic loading for a mild steel and a dual phase steel.

Key words: elasto-plasticity, time integration, constitutive algorithm.

1. INTRODUCTION

The finite element implementation of constitutive laws has observed considerable progress during the last two decades – partly due to the accelerated apparition of industrially-applied advanced materials, and of correspondingly complex constitutive models. Even a decade ago, three-year studies were typically dedicated to the finite element implementation of a particular, advanced model, which was fully exploited only several years after. Nowadays, there is a strong need for general constitutive algorithms allowing for rapid and modular implementation of material models which are under almost continuous improvement. Accordingly, various families of time integration schemes for material models have been recently proposed in the literature. In the framework of corotational algorithms established e.g. by [1] and others in the eighties, general and modular implicit algorithms were proposed [2, 3], which include an automatic procedure for the calculation of the algorithmic consistent tangent modulus. Explicit schemes [4, 5] have the advantage of robustness and simplicity of implementation, while requiring smaller time steps – which is suitable, for example, for dynamic explicit

Arts et Métiers ParisTech, LCFC, 4 rue A. Fresnel, 57078 Metz cedex 03, France

Ro. J. Techn. Sci. – Appl. Mechanics, Vol. 60, N^{os} 1–2, P. 89–104, Bucharest, 2015

simulations. Recent explicit schemes [6] claim improved accuracy. Both approaches have been illustrated on simple, isotropic damage models. Thermo-mechanical coupling in the FE simulation framework has also been tackled, mainly in the framework of bulk metal forming [7]; most time integration algorithms proposed in the literature are explicit [8, 9].

The current paper aims to review both the implicit and explicit time integration of elasto-plastic constitutive models, in view of their finite element implementation for forming process simulation, as well as material point simulations of selected strain paths for parameter identification. The paper is organized as follows. Section 2 recalls the equations of the constitutive model and further develops its discrete form over a loading increment and its numerical resolution. Section 3 describes the Runge-Kutta explicit time integration schemes as an effective means for the rapid implementation of advanced constitutive models. Algorithms are used to summarize the numerical methods through-out the paper. In Section 4, the proposed algorithms are applied to the simulation of a few non-monotonic strain-paths for two materials, for the sake of illustration.

2. CLASSICAL RATE-INDEPENDENT ELASTO-PLASTICITY

Rate-independent elasto-plasticity is considered in this paper as the reference material model. In this section, the equations of the constitutive model are recalled, along with their discrete counterparts, numerical resolution and corresponding algorithm. The constitutive equations are kept in generic form, so that any analytical yield function or hardening model can be incorporated easily. Further details on the time integration of hardening equations are given in Section 2.4.

2.1. ROTATION-COMPENSATED VARIABLES AND EQUATIONS

During forming, metals undergo large transformations and their behavior is described by rate constitutive equations. In order to respect the principle of objectivity, so-called objective derivatives must be used. In view of the numerical implementation of the models, a very attractive approach consists in writing these equations in an appropriate orthogonal rotating frame. The resulting equations are formally identical to their simpler, small-strain formulation, while verifying the objectivity principle at arbitrary strains. More explicitly, let $\mathbf{A}$ be a second order tensor, and let $\mathfrak{R}$ be an orthogonal rotation matrix. $\mathbf{A}$ and its objective derivative (designated by a superposed circle) can be written in a rotating frame generated by $\mathfrak{R}$ in the form

$$\hat{\mathbf{A}} = \mathfrak{R}^{\mathrm{T}}\mathbf{A}\mathfrak{R} \;; \qquad \dot{\hat{\mathbf{A}}} = \mathfrak{R}^{\mathrm{T}}\overset{o}{\mathbf{A}}\mathfrak{R}\,, \tag{1}$$

where the superposed hat designates quantities written in the rotating frame. In this particular frame, the objective derivative of any tensor **A** becomes its simple time derivative. The orthogonal rotation matrix $\mathfrak{R}$ can be generated by a skew-symmetric spin tensor $\boldsymbol{\Omega}$ using $\dot{\mathfrak{R}}\mathfrak{R}^{\mathrm{T}} = \boldsymbol{\Omega}$, where the superposed dot on $\mathfrak{R}$ indicates the time derivative, while $(\cdot)^{\mathrm{T}}$ designates the transpose of a tensor. On the other side, matrix $\mathfrak{R}$ must satisfy the objectivity condition under superimposed rigid-body motions. For example, Jaumann's derivative is obtained by setting $\boldsymbol{\Omega} = \mathbf{W}$, while the Green-Naghdi derivative is obtained with $\mathfrak{R} = \mathbf{R}$. Here, **W** denotes the total spin, while **R** is the orthogonal tensor in the polar decomposition of the deformation gradient.

In the following, all tensor variables are assumed to turn with the spin **W** (corresponding to the use of Jaumann rate), unless specified otherwise. Consequently, simple time derivatives are involved in the constitutive equations, making them form-identical to a small-strain formulation. For simplicity, the superposed hat (^) is omitted.

2.2. CONSTITUTIVE EQUATIONS

Classical rate-independent elasto-plastic models are described by the following set of equations:

- A hypo-elastic law (2) linearly relating the Cauchy stress rate $\dot{\boldsymbol{\sigma}}$ and the elastic strain rate $\mathbf{D}^e = \mathbf{D} - \mathbf{D}^p$;
- A yield function f and the corresponding plasticity criterion (3) bounding the elastic domain, and playing also the role of potential in stress space;
- A flow rule (4), defining the direction of the plastic strain rate $\mathbf{D}^p$ as the gradient of the yield function;
- A set of evolution laws (5) for the internal variables defining the hardening:

$$\dot{\boldsymbol{\sigma}} = \mathbf{C}^e : \left(\mathbf{D} - \mathbf{D}^p\right), \tag{2}$$

$$f(\boldsymbol{\sigma}, \mathbf{X}, \tau) = \bar{\sigma}(\mathbf{T}') - \tau \le 0, \tag{3}$$

$$\mathbf{D}^p = \dot{\lambda}\mathbf{V}; \quad \mathbf{V} = \frac{\partial f}{\partial \mathbf{T}}, \tag{4}$$

$$\dot{\mathbf{H}} = \dot{\lambda}\,\mathbf{h}(\mathbf{H}, \boldsymbol{\sigma}), \tag{5}$$

where:

- $\mathbf{C}^e$ is the elasticity constants fourth order tensor; in the case of linear isotropic elasticity $\mathbf{C}^e = 2G\,\mathbf{I}_4'^s + K\,\mathbf{I}\otimes\mathbf{I}$, with K and G being the bulk and shear elastic moduli, respectively, $\mathbf{I}$ is the second order unit tensor and $\mathbf{I}_4'^s$ the unit tensor in the space of fourth order symmetric deviatoric tensors, with components $I'^s_{4ijkl} = (1/2)(\delta_{ik}\delta_{jl} + \delta_{il}\delta_{jk}) - (1/3)\delta_{ij}\delta_{kl}$;
- τ is a scalar stress-type measure of the *size* of the yield surface, used to model isotropic hardening;
- $\mathbf{X}$ designates the backstress pointing to the *centre* of the yield surface, and thus describing the kinematic hardening;
- $\bar{\sigma}$ is the equivalent stress defining the *shape* of the yield surface;
- $\mathbf{T} = \boldsymbol{\sigma} - \mathbf{X}$ designates the so-called offset stress, whose deviator $\mathbf{T}'$ enters the equivalent stress expression;
- $\dot{\lambda}$ is the plastic multiplier, usually determined by enforcing the consistency condition $\dot{f} = 0$;
- $\mathbf{H} = (\tau, \mathbf{X}, ...)$ designates the complete set of internal variables of the considered hardening model.

2.3. DISCRETE EQUATIONS AND NUMERICAL RESOLUTION

The finite element implementation of such a constitutive model requires a time integration algorithm of the rate equations over the time interval $\Delta t = t_{n+1} - t_n$, when a total strain increment $\Delta\boldsymbol{\varepsilon}$ is imposed. The backward Euler time integration scheme is the most commonly used, and it consists in using the time derivatives at the end of the increment. In addition to a very good accuracy, this scheme was shown to be unconditionally stable with respect to the size of the strain increment, even with strongly non-linear material behaviors [10, 11]. The application of this scheme to the model above, in the case of plastic loading, leads to the following system of equations:

$$\text{Elasticity} \quad : \quad \Delta\boldsymbol{\sigma} - \mathbf{C} : \left(\Delta\boldsymbol{\varepsilon} - \Delta\boldsymbol{\varepsilon}^p\right) = \mathbf{0}, \tag{6}$$

$$\text{Normality} \quad : \quad \Delta\boldsymbol{\varepsilon}^p - \Delta\lambda\,\mathbf{V}_{n+1} = \mathbf{0}, \tag{7}$$

$$\text{Hardening} \quad : \quad \Delta\mathbf{H} - \Delta\lambda\,\mathbf{h}_{n+1} = \mathbf{0}, \tag{8}$$

$$\text{Yield function} \quad : \quad f_{n+1} = 0, \tag{9}$$

with unknowns $\boldsymbol{\varepsilon}^p_{n+1}$, λ_{n+1}, $\mathbf{H}_{n+1}$ and $\boldsymbol{\sigma}_{n+1}$. These equations can be solved directly by a Newton-Raphson method, as shown by Keavey [2,3]. The main limitation of such a direct resolution is related to the large size of the non-linear system to solve, leading to an increase in computing time and potentially to convergence issues. The size of the system can be reduced by applying substitutions and, in particular cases, by assuming that some of the internal variables can be treated in an uncoupled way. Most commonly, this leads to a nonlinear system of two equations, with unknowns $\Delta\lambda$ and $\mathbf{T}'_{n+1}$ [12]:

$$\begin{bmatrix} \mathbf{T}'_{n+1} + \Delta\lambda \mathbf{C}^e : \mathbf{V}\left(\mathbf{T}'_{n+1}\right) + \Delta\mathbf{X}(\Delta\lambda, \mathbf{T}'_{n+1}) - \mathbf{T}'_n - \mathbf{C}^e : \Delta\boldsymbol{\varepsilon}' \\ \bar{\sigma}\left(\mathbf{T}'_{n+1}\right) - \tau\left(\Delta\lambda, \mathbf{T}'_{n+1}\right) \end{bmatrix} = \begin{bmatrix} \mathbf{0} \\ 0 \end{bmatrix}. \tag{10}$$

The size of this system is independent of the number of internal variables, thus representing a beneficial compromise between accuracy, robustness and computing cost. At each time increment, this nonlinear equation system is solved using a classical numerical method, for example the well known Newton-Raphson algorithm. It is noteworthy that the size of the system can be further reduced to two scalar equations in the case of Hill's quadratic yield function, and to a single scalar equation (with unknown $\Delta\lambda$) for von Mises. Here, the form (10) is kept for generality, so that arbitrary anisotropic yield function can be incorporated.

In view of the implementation in an implicit finite element code, an algorithmic tangent modulus must also be calculated, consistently with the adopted time integration scheme. For the time integration scheme adopted here, the tangent modulus can be written in the form [13]

$$\mathbf{C}^{\text{alg}} = \frac{D(\Delta\boldsymbol{\sigma})}{D(\Delta\boldsymbol{\varepsilon})} = K\mathbf{I}\otimes\mathbf{I} + 2G\mathbf{I}'^s_4 - 4\alpha G^2 \left[\left(\frac{\partial\tau}{\partial\Delta\lambda} \right)^{-1} \mathbf{V} \otimes \left(\mathbf{V} - \frac{\partial\tau}{\partial\mathbf{T}'} \right) + \Delta\lambda\mathbf{Q} \right] : \boldsymbol{\Lambda}^{-1} \tag{11}$$

where $\alpha=1$ in the elasto-plastic case, and $\alpha=0$ in the elastic case; $\mathbf{Q}$ represents the second order derivative of the equivalent stress, and

$$\boldsymbol{\Lambda} = \mathbf{I}'^s_4 + 2G \left[\left(\frac{\partial\tau}{\partial\Delta\lambda} \right)^{-1} \mathbf{V} \otimes \left(\mathbf{V} - \frac{\partial\tau}{\partial\mathbf{T}'} \right) + \Delta\lambda\mathbf{Q} \right] + \frac{\partial\mathbf{X}}{\partial\mathbf{T}'} + \left(\frac{\partial\tau}{\partial\Delta\lambda} \right)^{-1} \frac{\partial\mathbf{X}}{\partial\Delta\lambda} \otimes \left(\mathbf{V} - \frac{\partial\tau}{\partial\mathbf{T}'} \right).$$

2.4. ON THE TIME INTEGRATION OF HARDENING EQUATIONS

The algorithms discussed in this paper are generic and may be applied to various particular cases of yield function and hardening equations. Concerning the yield function, one needs to calculate its first and second derivatives to feed the algorithm. For the hardening equations (5), one needs to calculate their incremental

form (8) where the backward Euler scheme is consistently used. However, analytical or semi-analytical [14] time integrations are often possible and offer an accurate alternative. For example, the saturating laws of Voce (for isotropic hardening) and Armstrong-Fredericks (for kinematic hardening) can be integrated as follows:

$$\dot{R} = C_R\left(R_{\text{sat}} - R\right)\dot{\lambda} \quad \rightarrow \quad \mathrm{R}_{n+1} = R_{\text{sat}} - \left(R_{\text{sat}} - R_n\right)e^{-C_R\Delta\lambda}, \tag{12}$$

$$\dot{\mathbf{X}} = C_X\left(X_{\text{sat}}\mathbf{N} - \mathbf{X}\right)\dot{\lambda} \quad \rightarrow \quad \mathbf{X}_{n+1} = X_{\text{sat}}\mathbf{N}_{n+1} - \left(X_{\text{sat}}\mathbf{N}_{n+1} - \mathbf{X}_n\right)e^{-C_X\Delta\lambda}, \tag{13}$$

where $\mathbf{N}$ designates the direction of the plastic strain rate tensor. Note that the condition $\mathbf{N} \equiv \mathbf{N}_{n+1}$ was needed to allow for the analytical integration of the backstress $\mathbf{X}$. This is not an additional approximation, but is a consequence of the usage of the backward Euler integration of the plastic strain (7) over the increment. With this statement in mind, numerous particular hardening equations accept such closed-form semi-analytical alternative forms. As an illustration, Fig. 1 compares the analytical and the backward Euler time integrations for Eq. (12).

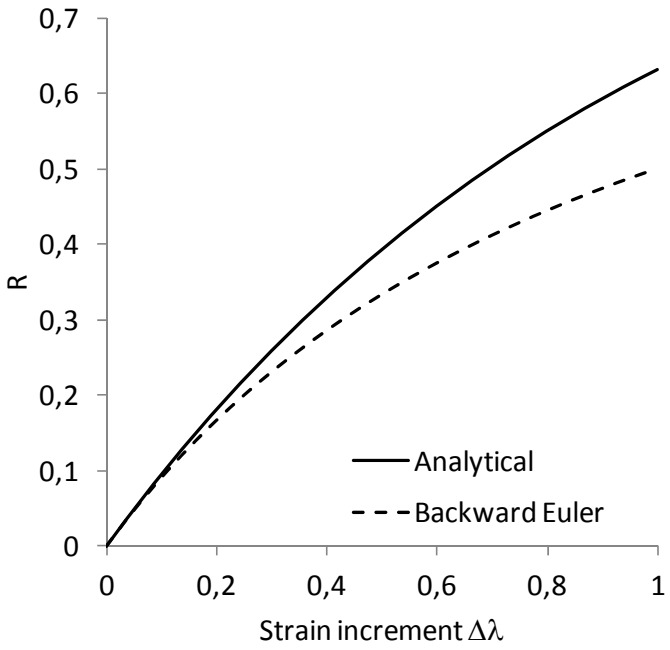

Fig. 1 – Influence of the increment size on the accuracy of the time integration of Voce's isotropic hardening equation. Parameters $R_{\text{sat}}=C_R=1$ were used.

2.5. TIME INTEGRATION ALGORITHM

To close this section, the time integration scheme along with the numerical resolution of the resulting equations are summarized in algorithmic form in Algorithm 1.

Algorithm 1 – Implicit time integration of the elasto-plastic constitutive model.

Input: $\Delta\boldsymbol{\varepsilon}$, $\boldsymbol{\sigma}_n$ and $\mathbf{H}_n$

Elastic trial stress: $\boldsymbol{\sigma}_{n+1}^{\text{try}} = \boldsymbol{\sigma}_n + \mathbf{C} : \Delta\boldsymbol{\varepsilon}$

Calculate $f_{n+1}^{\text{try}} = \bar{\sigma}\left(\boldsymbol{\sigma}_{n+1}'^{\text{try}} - \mathbf{X}_{n+1}\right) - \tau\left(\mathbf{H}_{n+1}\right)$

If $f_{n+1}^{\text{try}} < 0$, elastic increment:

State update: $\boldsymbol{\sigma}_{n+1} = \boldsymbol{\sigma}_{n+1}^{\text{try}}$; $\mathbf{H}_{n+1} = \mathbf{H}_n$

Else, elastic-plastic increment:

Initialization: $\mathbf{T}'_{n+1} = \boldsymbol{\sigma}_{n+1}'^{\text{try}} - \mathbf{X}_n$; $\Delta\lambda = 0$

Compute $\mathbf{T}'_{n+1}$ and $\Delta\lambda$: solve (10) by the Newton-Raphson method

State update: $\mathbf{H}_{n+1} = \mathbf{H}\left(\mathbf{T}_{n+1}, \Delta\lambda\right)$ according to hardening model

$\boldsymbol{\sigma}_{n+1} = \mathbf{T}_{n+1} + \mathbf{X}_{n+1}$

Compute algorithmic tangent modulus $\mathbf{C}^{\text{Algo}}$ with Eq. (11)

End of algorithm; output: $\boldsymbol{\sigma}_{n+1}$, $\mathbf{C}^{\text{Algo}}$, updated internal variables

3. EXTENSIONS TO MORE COMPLEX BEHAVIOR LAWS

In the context of the constitutive model adopted in Section 2, one can adopt specific forms of the yield function or hardening model, in order to describe particular types of metallic materials. From the numerical viewpoint, first and second order derivatives must be calculated for these models in order to allow for the numerical resolution with the implicit time integration scheme. The proposed modeling framework also allows for further extensions to cover wider ranges of metallic materials, for example during forming. In many cases, the strain-rate sensitivity of the metallic materials cannot be neglected – for example if strain localization needs to be modeled accurately. Additional terms and equations are included in the material model, modifying the numerical algorithm. The additional numerical developments required for such extensions are one of the bottlenecks for advanced material models to be adopted in industrial applications. An alternative solution to this problem is offered by explicit time integration schemes. The main

drawback of explicit time integration is related to its conditional stability, requiring smaller time steps that for implicit integration. This drawback is significantly reduced for problems involving contact and plasticity, where relatively small loading increments are required anyway. In turn, the numerical development is much faster, does not require additional derivative calculations, and does not need convergence loops. In this section, a formal algorithm is proposed for the explicit time integration of elasto-plastic material models. Then, this algorithm is used to solve an example of more complex constitutive model for multiphase materials.

3.1. EXPLICIT TIME INTEGRATION

The explicit time integration of equations (2)-(5) makes use of the values of the state variables at time t_n when deriving the discrete equations (6)-(9). Consequently, the resulting equations are explicit and the state at t_{n+1} can be determined without any iteration. The accuracy of the method can be improved by adopting higher order Runge-Kutta integration schemes. The corresponding algorithm reduces to a loop of order $N=1$, 2 or 4 (for Euler explicit, Runge-Kutta order 2 or Runge-Kutta order 4) with the same contents. Moreover, the algorithmic tangent modulus is recovered by a simple summation of the N tangent moduli [13].

In contrast to the implicit time integration, the loading-unloading condition cannot be based on the value of the yield function alone, since a plastic state at the beginning of the increment may still be followed by elastic unloading. Robust loading-unloading conditions are obtained by checking the orientation of the total strain increment with respect to the normal to the current yield surface, as shown in Fig. 2. Algorithm 2 summarizes the Runge-Kutta explicit time integration of elasto-plastic models.

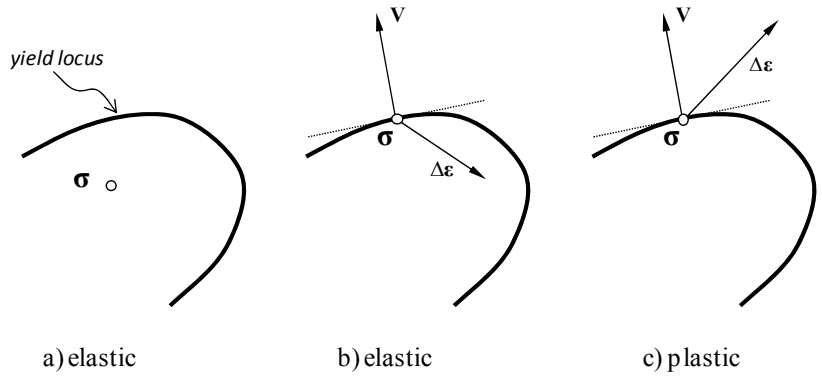

Fig. 2 – Schematic illustration of loading–unloading conditions in the framework of an explicit time integration algorithm, given a stress state $\boldsymbol{\sigma}$ and a loading increment $\Delta\boldsymbol{\varepsilon}$.

Algorithm 2 – Runge-Kutta explicit time integration of the elasto-plastic constitutive model.

Input: $\Delta\boldsymbol{\varepsilon}$, $\boldsymbol{\sigma}_n$ and $\mathbf{H}_n$

Initialization: $\Delta\boldsymbol{\sigma}_0 = \mathbf{0}$; $\Delta\mathbf{H}_0 = \mathbf{0}$

Calculate, for i = 1 to N:

Compute $\boldsymbol{\sigma}_i = \boldsymbol{\sigma}_n + a_i \Delta\boldsymbol{\sigma}_{i-1}$; $\mathbf{H}_i = \mathbf{H}_n + a_i \Delta\mathbf{H}_{i-1}$

Compute $f_i\left(\boldsymbol{\sigma}_i, \mathbf{H}_i\right) = \bar{\sigma}\left(\boldsymbol{\sigma}_i' - \mathbf{X}_i\right) - \tau\left(\mathbf{H}_i\right)$

Compute $\beta_i = \Delta\boldsymbol{\varepsilon} : \mathbf{V}_i$

If $f_i < 0$ or $\beta_i < 0$, elastic increment:

Compute $\Delta\boldsymbol{\sigma}_i = \mathbf{C} : \Delta\boldsymbol{\varepsilon}$; $\Delta\mathbf{H}_i = \mathbf{0}$; $\mathbf{C}_i^{\text{Algo}} = \mathbf{C}$

Else, elasto-plastic increment:

Compute $\mathbf{V}_i = \left.\dfrac{\partial f}{\partial \boldsymbol{\sigma}}\right|_i$; $\Delta\lambda_i = \dfrac{\mathbf{V}_i : \mathbf{C} : \Delta\boldsymbol{\varepsilon}}{\mathbf{V}_i : \mathbf{C} : \mathbf{V}_i + \mathbf{V}_i : \mathbf{h}_{Xi} + h_{\tau i}}$

Compute $\Delta\boldsymbol{\varepsilon}_i^p = \mathbf{V}_i \Delta\lambda_i$

Compute $\Delta\boldsymbol{\sigma}_i = \mathbf{C} : \left(\Delta\boldsymbol{\varepsilon} - \Delta\boldsymbol{\varepsilon}_i^p\right)$; $\Delta\mathbf{H}_i = \Delta\lambda_i \mathbf{h}\left(\boldsymbol{\sigma}_i, \mathbf{H}_i\right)$

Compute $\mathbf{C}_i^{\text{Algo}} = \mathbf{C} - \dfrac{\left(\mathbf{C} : \mathbf{V}_i\right) \otimes \left(\mathbf{V}_i : \mathbf{C}\right)}{\mathbf{V}_i : \mathbf{C} : \mathbf{V}_i + \mathbf{V}_i : \mathbf{h}_{Xi} + h_{\tau i}}$

Update state variables: $\boldsymbol{\sigma}_{n+1} = \boldsymbol{\sigma}_n + \sum_{i=1}^{N} b_i \Delta\boldsymbol{\sigma}_i$; $\mathbf{H}_{n+1} = \mathbf{H}_n + \sum_{i=1}^{N} b_i \Delta\mathbf{H}_i$

Compute consistent tangent modulus: $\mathbf{C}^{\text{Algo}} = \sum_{i=1}^{N} b_i \mathbf{C}_i^{\text{Algo}}$

End of algorithm; output: $\boldsymbol{\sigma}_{n+1}$, $\mathbf{C}^{\text{Algo}}$, updated internal variables

3.2. EXAMPLE OF APPLICATION TO MULTIPHASE STEELS

Multiphase steels are used here as an example of constitutive model of increased complexity, while remaining in the framework of macroscopic modeling. In Dual-Phase or Complex-Phase steels, each of the N_φ constitutive phases (martensite, ferrite, etc.) can be described by a specific model of the type described in Section 2.2. A possible approach to describe the overall constitutive behavior consists in adopting a homogenization method to build the global response based on the response of each constituent and the corresponding volume fractions f^φ, $\varphi = \overline{1, N^\varphi}$ as

$$\boldsymbol{\sigma} = \sum_{\varphi=1}^{N^{\varphi}} f^{\varphi}\boldsymbol{\sigma}^{\varphi} \; ; \qquad \mathbf{D} = \sum_{\varphi=1}^{N^{\varphi}} f^{\varphi}\mathbf{D}^{\varphi} . \tag{14}$$

Given the total strain rate tensor **D**, the corresponding strain rate tensors in each phase are determined by means of a so-called localization rule

$$\mathbf{D}^{\varphi} = \mathbf{A}^{\varphi}\mathbf{D} , \tag{15}$$

where the fourth order tensors $\mathbf{A}^{\varphi}$ are function of the state variables and their expressions differ from one homogenization method to another (see, e.g, [15]). For each phase φ, the relationship between $\boldsymbol{\sigma}^{\varphi}$ and $\mathbf{D}^{\varphi}$ is governed by equations (2)-(5) with a specific set of material parameters each.

Specific implicit time integration schemes can be developed for such complex models. However, the framework of explicit time integration algorithms allows for a straightforward and modular implementation that directly incorporates Algorithm 2 as a module – see Algorithm 3. Usually, the number of predictor-corrector loops can be bounded to a fixed maximum value. Similar explicit time integration schemes have also been applied when enhancing the constitutive model with strain-rate sensitivity [16], microstructure-related internal variables [17], or damage [18].

4. SIMULATION OF HOMOGENEOUS RHEOLOGICAL TESTS

Algorithms 1-3 can be implemented in a non-linear finite element code, in order to predict the non-linear behavior of metallic structures during plastic deformation. Homogeneous rheological tests, used to emphasize the model predictions under typical loading histories, can be simulated with single element models. Alternatively, a time marching algorithm can be developed to impose selected kinematics to a material point. In this section, such a time-marching algorithm is described which proved very efficient, for example, in view of the parameter identification of material models.

Algorithm 3 – Time integration of the elasto-plastic model for multiphase materials.

Input: $\Delta\boldsymbol{\varepsilon}$, $\boldsymbol{\sigma}_n^{\varphi}$, $\mathbf{H}_n^{\varphi}$, $\varphi = \overline{1, N^{\varphi}}$; material parameters

Initialization: $\boldsymbol{\sigma}_{n+1}^{\varphi} \leftarrow \boldsymbol{\sigma}_n^{\varphi}$, $\mathbf{H}_{n+1}^{\varphi} \leftarrow \mathbf{H}_n^{\varphi}$

Beginning of convergence loop

For each phase $\varphi = \overline{1, N^{\varphi}}$:

Calculate $\mathbf{A}^{\varphi}$ based on current state variables

Calculate $\Delta\boldsymbol{\varepsilon}^{\varphi} = \mathbf{A}^{\varphi}\Delta\boldsymbol{\varepsilon}$

Update $\boldsymbol{\sigma}_{n+1}^{\varphi}, \mathbf{H}_{n+1}^{\varphi}, \mathbf{C}_{\text{algo}}^{\varphi}$ – use Algorithm 2

Calculate $\boldsymbol{\sigma}_{n+1} = \sum_{\varphi=1}^{N^{\varphi}} f^{\varphi}\boldsymbol{\sigma}_{n+1}^{\varphi}$

Repeat loop until $\sum_{\varphi=1}^{N^{\varphi}} f^{\varphi}\Delta\boldsymbol{\varepsilon}^{\varphi} \approx \Delta\boldsymbol{\varepsilon}$, within a selected tolerance

Calculate $\mathbf{C}_{\text{algo}} = \sum_{\varphi=1}^{N^{\varphi}} f^{\varphi}\mathbf{C}_{\text{algo}}^{\varphi}$

End of algorithm; output: $\boldsymbol{\sigma}_{n+1}$, $\mathbf{C}_{\text{algo}}$, $\boldsymbol{\sigma}_{n+1}^{\varphi}$, updated internal variables per phase

The kinematics of a material point is completely defined by the deformation gradient $\mathbf{F}$ as a function of time, or alternatively its rate $\dot{\mathbf{F}}$. This loading history needs to be split in time increments, and some kinematical assumption must be adopted over an increment. Hughes [1] proposed to assume that the displacement of material points varies linearly over the time increment. Thus, at a time $t_{\alpha} = t_n + \alpha\Delta t$ during the loading increment $\mathbf{x}_{\alpha} = (1-\alpha)\mathbf{x}_n + \alpha\mathbf{x}_{n+1}$, with $\alpha = [0,1]$. Consequently, a displacement gradient $\mathbf{G}_{\alpha} = \partial(\mathbf{x}_{n+1} - \mathbf{x}_n)/\partial\mathbf{x}_{\alpha}$ can be calculated in terms of $\mathbf{F}_n$ and $\mathbf{F}_{n+1}$. The strain and spin increments $\Delta\boldsymbol{\varepsilon}$ and $\Delta\mathbf{W}$ are calculated as the symmetric and skew-symmetric parts of $\mathbf{G}_{\alpha}$, respectively. The most accurate results are obtained for α=1/2; the corresponding displacement gradient is calculated using the mid-point deformation gradient $\mathbf{F}_{1/2} = \frac{1}{2}(\mathbf{F}_n + \mathbf{F}_{n+1})$.

Another approximation has to be made when the strain increment is computed, since the material frame rotates during the time increment. Reference [1] suggests to provide the time integration algorithm with the strain increment rotated in a mid-point orientation as $\Delta\hat{\boldsymbol{\varepsilon}} = \mathfrak{R}_{1/2}^{\mathrm{T}}\,\Delta\boldsymbol{\varepsilon}\,\mathfrak{R}_{1/2}$. If the rotation is calculated by polar decomposition (Green-Naghdi objective derivative), $\mathfrak{R}_{1/2} \equiv \mathbf{R}_{1/2}$ is calculated based on the min-point deformation gradient. In the case of Jaumann's

derivative, $\mathfrak{R}_{1/2} = \Delta\mathfrak{R}^{1/2}\mathfrak{R}_n$ where the incremental rotation $\Delta\mathfrak{R}$ over the time increment is determined as

$$\Delta\mathfrak{R} = \mathbf{I} + \left(\mathbf{I} - \frac{1}{2}\Delta\mathbf{W}\right)^{-1}\Delta\mathbf{W}. \tag{16}$$

In Fig. 3, this choice of incremental kinematics is validated against the analytical solution for the case of simple shear, which combines large strains and large rotations. The non-zero components of the rotated strain increment are plotted, as calculated via single-increment simulations with increasing shear loading increments. The accuracy of the incremental kinematics is excellent up to very large increment values ($\Delta\gamma = 100\%$).

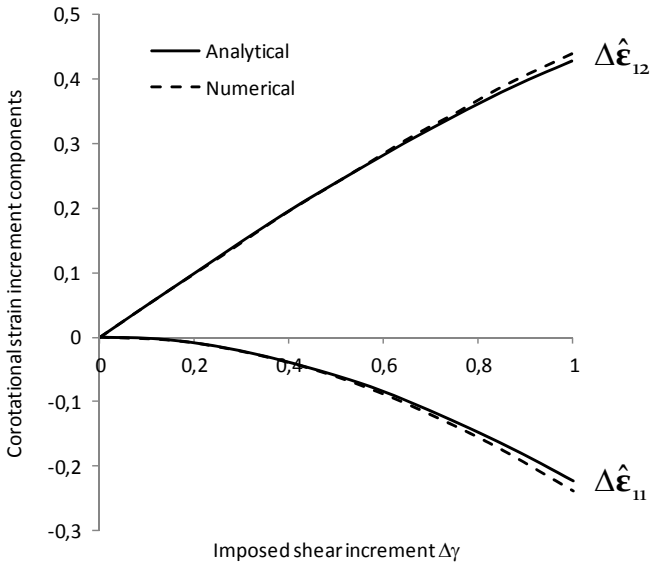

Fig. 3 – Influence of the increment size on the accuracy of the co-rotational strain increment.

The complete algorithm that implements this approach for the simulation of homogeneous (material point) loading modes is given in Algorithm 4. This algorithm may serve for the stand-alone simulation of mechanical tests, or it can be implemented in a finite element software in order to provide user control over the incremental kinematics. The algorithm is detailed for Jaumann's derivative, but the implementation for Green-Naghi is similar. Following Mandel's pioneering work on the average plastic spin of polycrystals [19], phenomenological models have been proposed to describe the evolution of the plastic spin (see, e.g., [20–22]), as well as the corresponding computer implementation algorithms [23, 24]; this

extension can also be implemented in Algorithm 4 with minor modifications. If a finite element implementation is performed, the algorithmic tangent algorithm needs also to be rotated in the global frame at the end of the algorithm (see, e.g., [25]).

Figure 4 illustrates the application of this algorithm to the prediction of sequential homogeneous rheological tests using the constitutive model of Teodosiu and Hu [26, 27]. This model makes use of four internal variables, including two second-order and one fourth-order tensors, to describe complex strain-path change phenomena as observed in the figure. The simulation of such sequential two-step strain paths with stand-alone algorithms independent of a finite element software is required for the efficient parameter identification of such model [28, 29].

Algorithm 4 – Time integration of elasto-plastic constitutive models in the fixed frame, including the incremental kinematics.

Input: $\mathbf{F}_0$, $\dot{\mathbf{F}}$(constant), Δt, t_{end}, $\boldsymbol{\sigma}_0$, $\mathbf{H}_0$, $\mathfrak{R}_0$, material parameters

$n = 0$

Calculate, for $t = 0$ to t_{end}, step Δt :

Kinematics:

Compute $\Delta\mathbf{F} = \dot{\mathbf{F}}\Delta t$; $\mathbf{F}_{n+1} = \mathbf{F}_n + \Delta\mathbf{F}$; $\mathbf{F}_{1/2} = \frac{1}{2}\left(\mathbf{F}_n + \mathbf{F}_{n+1}\right)$

Compute $\Delta\mathbf{G}_{1/2} = \Delta\mathbf{F}\cdot\mathbf{F}_{1/2}^{-1}$; $\Delta\boldsymbol{\varepsilon} = \Delta\mathbf{G}_{1/2}^{\text{sym}}$; $\Delta\mathbf{W} = \Delta\mathbf{G}_{1/2}^{\text{skew}}$

Compute $\Delta\mathfrak{R} = \mathbf{I} + \left(\mathbf{I} - \frac{1}{2}\Delta\mathbf{W}\right)^{-1}\Delta\mathbf{W}$; $\Delta\mathfrak{R}_{1/2} = \left(\Delta\mathfrak{R}\right)^{1/2}$

Compute $\mathfrak{R}_{n+1} = \Delta\mathfrak{R}\cdot\mathfrak{R}_i$; $\mathfrak{R}_{1/2} = \Delta\mathfrak{R}_{1/2}\cdot\mathfrak{R}_i$

Rotation to material frame:

Compute $\hat{\boldsymbol{\sigma}}_n = \mathfrak{R}_n^{\mathrm{T}}\boldsymbol{\sigma}_n\mathfrak{R}_n$ (apply to all tensorial internal variables)

Compute $\Delta\hat{\boldsymbol{\varepsilon}} = \mathfrak{R}_{1/2}^{\mathrm{T}}\Delta\boldsymbol{\varepsilon}\,\mathfrak{R}_{1/2}$

State update:

Compute $\hat{\boldsymbol{\sigma}}_{n+1}, \hat{\mathbf{H}}_{n+1}$, tangent modulus (use Algorithms 1, 2 or 3)

Rotation back to fixed frame:

Compute $\boldsymbol{\sigma}_{n+1} = \mathfrak{R}_{n+1}\hat{\boldsymbol{\sigma}}_{n+1}\mathfrak{R}_{n+1}^{\mathrm{T}}$ (+ all tensorial internal variables)

Initialize next increment:

$n \leftarrow n+1$

$\left(\boldsymbol{\sigma}_{n+1}, \mathbf{H}_{n+1}, \mathfrak{R}_{n+1}, \mathbf{F}_{n+1}\right) \leftarrow \left(\boldsymbol{\sigma}_n, \mathbf{H}_n, \mathfrak{R}_n, \mathbf{F}_n\right)$

End of loop

End of algorithm

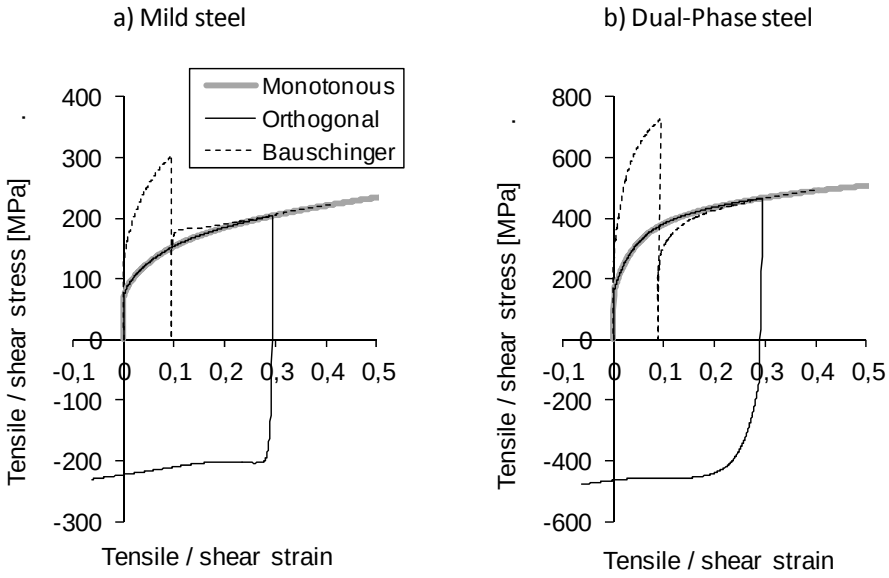

Fig. 4 – Rheological simulation of monotonic shear, reverse shear (Bauschinger) and tension followed by shear in the same direction (Orthogonal). Material parameters from [30] corresponding to two classical forming steel grades.

Acknowledgements. The author is grateful to C. Teodosiu for his scientific guidance and fruitful discussions and support in the field of constitutive modeling and the associated computational problems and developments, during many years.

Received on July 16, 2015

REFERENCES

1. HUGHES, T.J.R., *Numerical implementation of constitutive models: rate-independent deviatoric plasticity*, in: *Theoretical foundations for large-scale computations for non-linear material behavior* (eds. S. Nemat-Nasser *et al*.), Martinus Nijhoff Publishers, Dordrecht, The Netherlands, 1984, pp. 29–57.
2. KEAVEY, M.A., *A canonical form return mapping algorithm for rate independent plasticity*, Int. J. Num. Meth. Eng., **53**, *6*, pp. 1491–1510, 2002.
3. KEAVEY, M.A., *A simplified canonical form algorithm with application to porous metal plasticity*, Int. J. Num. Meth. Eng., **65**, *5*, pp. 679–700, 2006.
4. SLOAN, S., ABBO, A., SHENG, D., *Refined explicit integration of elastoplastic models with automatic error control*, Engineering Computations, **18**, *1–2*, pp. 121–154, 2001.
5. DING, K.Z., QIN, Q.H., CARDEW-HALL, M., *Substepping algorithms with stress correction for the simulation of sheet metal forming process*, International Journal of Mechanical Sciences, **49**, *11*, pp. 1289–1308, 2007.
6. VRH, M. , HALILOVIČ, M. , ŠTOK, B., *Improved explicit integration in plasticity*, Int. J. Num. Meth. Eng., **81**, *7*, pp. 910–938, 2010.

7. KOJIC, M., BATHE, K.J., *The 'effective-stress-function' algorithm for thermo-elasto-plasticity and creep*, Int. J. Num. Meth. Eng., **24**, *8*, pp. 1509–1532, 1987.
8. MICARI, F., FRATINI, L., ALBERTI, N., *An explicit model for the thermal-mechanical analysis of hot metal forming processes*, Annals of the CIRP, **44**, *1*, pp. 193–196, 1995.
9. BERGMAN, G., OLDENBURG, M., *A finite element model for thermomechanical analysis of sheet metal forming*, Int. J. Num. Meth. Eng., **59**, *9*, pp. 1167–1186, 2004.
10. SIMO, J., TAYLOR, R., *Consistent tangent operators for rate-independent elasto-plasticity*. Computer Methods in Applied Mechanics and Engineering, **48**, *1*, pp. 101–118, 1985.
11. ORTIZ, M., POPOV, E.P., *Accuracy and stability of integration algorithms for elastoplastic constitutive relations*, Int. J. Num. Meth. Eng., **21**, *9*, pp. 1561–1576, 1985.
12. ALVES, J.L., *Simulação numérica do processo de estampagem de chapas metálicas: Modelação mecânica e métodos numéricos*, PhD Thesis, University of Minho, Portugal, 2003.
13. HADDAG, B, *Contribution to the modeling of sheet metal forming: application to springback and localization*, PhD Thesis, ENSAM Metz, France, 2007.
14. CHABOCHE, J.L., CAILLETAUD, G., *Integration methods for complex plastic constitutive equations*, Computer Methods in Applied Mechanics and Engineering, **133**, *1–2*, pp. 125–155, 1996.
15. BERVEILLER, M., ZAOUI, A., *An extension of the self-consistent scheme to plastically-flowing polycrystals*, J. Mech. Phys. Sol., **26**, *5–6*, pp. 325–344, 1978.
16. PIPARD, J.M., BALAN, T., ABED-MERAIM, F., LEMOINE, X., *Elasto-visco-plastic modeling of mild steels for sheet forming applications over a large range of strain rates*, International Journal of Solids and Structures, **50**, *16–17*, pp. 2691–2700, 2013.
17. RESENDE, T.C., BALAN, T., BOUVIER, S., ABED-MERAIM, F., SABLIN, S.S., *Numerical investigation and experimental validation of a plasticity model for sheet steel forming*, Modelling and Simulation in Materials Science and Engineering, **21**, *1*, doi:10.1088/0965-0393/21/1/015008, 2013.
18. FANSI, J., BALAN, T., LEMOINE, X., MAIRE, E., LANDRON, C., BOUAZIZ, O., BEN BETTAIEB, M., HABRAKEN, A.M., *Numerical investigation and experimental validation of physically-based advanced GTN model for DP steels*, Materials Science and Engineering A, **569**, pp. 1–12, 2013.
19. MANDEL, J., *Définition d'un repère privilégié pour l'étude des transformations anélastiques du polycristal*, Journal de Mécanique Théorique et Appliquée, **1**, pp. 7-23, 1982.
20. KURODA, M., *Interpretation of the behavior of metals under large plastic shear deformations: a macroscopic approach*, International Journal of Plasticity, **13**, *4*, pp. 359-383, 1997.
21. PEETERS, B., HOFERLIN, E., VAN HOUTTE, P., AERNOUDT, E., *Assessment of crystal plasticity based calculation of the lattice spin of polycrystalline metals for FE implementation*, International Journal of Plasticity, **17**, *6*, pp. 819–836, 2001.
22. DAFALIAS, Y.F., *Plastic spin: necessity or redundancy*, International Journal of Plasticity, **14**, *9*, pp. 909–931, 1998.
23. HAN, C.S., CHOI, Y., LEE, J.K., WAGONER, R.H., *A FE formulation for elasto-plastic materials with planar anisotropic yield functions and plastic spin*, International Journal of Solids and Structures, **39**, *20*, pp. 5123–5141, 2002.
24. DUCHÊNE, L., LELOTTE, T., FLORES, P., BOUVIER, S., HABRAKEN, A.M., *Rotation of axes for anisotropic metal in FEM simulations*, International Journal of Plasticity, **24**, *3*, pp. 397–427, 2008.
25. SALAHOUELHADJ, A., ABED-MERAIM, F., CHALAL, H., BALAN, T., *Implementation of the continuum shell finite element SHB8PS for elastic-plastic analysis and application to sheet forming simulation*, Archive of Applied Mechanics, **82**, *9*, pp. 1269–1290, 2012.
26. TEODOSIU, C., HU, Z., *Evolution of the intragranular microstructure at moderate and large strains: Modeling and computational significance*. in: *Simulation of Materials Processing: Theory, Methods and Applications. Numiform'95 Proceedings*, 1995, pp. 173–182.

27. HADDAG, B, BALAN, T., ABED-MERAIM, F., *Investigation of advanced strain-path dependent material models for sheet metal forming simulations*, International Journal of Plasticity, **23**, *6*, pp. 951–979, 2007.
28. HADDADI, H., BOUVIER, S., BANU, M., MAIER, C., TEODOSIU, C., *Towards an accurate description of the anisotropic behaviour of sheet metals under large plastic deformations: Modelling, numerical analysis and identification*, International Journal of Plasticity, **22**, *12*, pp. 2226–2271, 2006.
29. YIN, Q., TEKKAYA, A.E., TRAPHÖNER, H., *Determining cyclic flow curves using the in-plane torsion test*, CIRP Annals – Manufacturing Technology, **64**, *1*, pp. 261–264, 2015.
30. BOUVIER, S., ALVES, J.L., OLIVEIRA, M.C., MENEZES, L.F., *Modeling of anisotropic work-hardening behavior of metallic materials subjected to strain-path changes*, Computational Material Science, **32**, *3–4*, pp. 301–315, 2005.